Implementation of a damage-plasticity DEM contact model in PFC3d.

Jinhui Zheng & Matteo Oryem Ciantia, University of Dundee, m.o.ciantia@dundee.ac.uk

A new plasticity bond damage model for highly porous, soft rocks is proposed and implemented as a contact model in the discrete element method DEM. The Particle upscaling law for strength, softening and far-field interaction parameters are presented and validated in Zheng & Ciantia (2025) enabling computational efficiency. Also, a strength correction equation is developed in Zheng & Ciantia (2025) to consider sample size effect of rocks. Finally, for boundary value problems like pile installation, the computational improvement of the model led pile penetration simulations in porous, soft rocks for the first time conducted in Zheng & Ciantia (2025).

Model description:

There are two types of contact forces, bonded and unbonded forces, induced by bonded and unboned physical contacts in the model, respectively.

For bonded contact forces, they are calculated as follows:

$$\begin{bmatrix} N \\ V \\ \breve{M} \end{bmatrix} = \begin{bmatrix} k_n(u_n - u_n^p)A \\ k_s(u_s - u_s^p)A \\ k_b(\theta_b - \theta_b^p)/\bar{R} \end{bmatrix} = \begin{bmatrix} (1-D)k_n^0(u_n - u_n^p)A \\ (1-D)k_s^0(u_s - u_s^p)A \\ (1-D)k_b^0(\theta_b - \theta_b^p)/\bar{R} \end{bmatrix} \quad (1)$$

With N and V being the normal and shear forces on the bond; $\breve{M}$ is the bending moment on the bond normalized by the bond radius $\bar{R}$; A is the cross-sectional area of the bond; D is an internal variable of the bond representing its level of damage, its value varies from 0 (intact) to 1 (broken); k_n^0 and k_s^0 are the initial normal and shear stiffness; k_b^0 is the initial bending stiffness, $k_b^0 = k_n^0 I$, I is the inertia moment of the bond. . u_n and u_s (the normal and shear displacement of the bond, respectively) and θ_b (the relative bond rotation) are subdivided into elastic and plastic components, where superscripts e and p correspond to the elastic and plastic (irreversible) parts, respectively.

Following Nguyen et al. (2017) bond damage evolution can be framed as:

$$D = 1 - exp^{-\left(\frac{|u_n^p|}{u^c} + \frac{u_s^p}{u^c} + \frac{\theta_b^p}{\theta^c}\right)} \quad (2)$$

u^c and θ^c are parameters controlling the softening rate and are related to the fracture energies of the bond for the respective loading regime. The absolute value of the normal plastic displacement is used to account for damage in both tension and compression.

The above equations describe elastic behaviour of bonds within the 3D yield surface expressed by the following equation f :

$$f = \left(\frac{\widetilde{M}}{\overline{\widetilde{M}}}\right)^{1.001} + \left(\frac{N}{\overline{N}}\right)^2 + \left(\frac{V}{\overline{V}}\right)^4 \left[1 - \left(\frac{N}{\overline{N}}\right)^2\right]^{-1} - 1 \tag{3}$$

Where, the size of the fielding domain is controlled by the bond strength parameters $\widetilde{M}, \overline{N}$ and $\overline{V}$ that decrease linearly with the level of bond damage D:

$$\begin{bmatrix} \overline{N} \\ \overline{V} \\ \overline{\widetilde{M}} \end{bmatrix} = \begin{bmatrix} \overline{N} \\ \overline{V} \\ \overline{M}/\overline{R} \end{bmatrix} = \begin{bmatrix} \sigma_0 A \\ CA \\ \sigma_t I/\overline{R}^2 \end{bmatrix} (1 - D) \tag{4}$$

σ_0 and C are the normal and shear strengths, respectively. $\sigma_0 = \sigma_t$ under tension and $\sigma_0 = \sigma_c$ under compression, σ_t and σ_c are the tensile and compressive strength of the bond. The 3D yield surface hence gradually shrinks with increasing bond damage until the bond failure ($D = 1$). To evaluate plastic behaviour of the bond, a traditional plastic mechanics related to associate flow rule is employed to calculate plastic deformation of bonds. More details can be found in Zheng & Ciantia (2025).

For unbonded forces, they are incrementally updated in a linear law, governed by two elastic parameters (E_{mod}, κ^*), with the interparticle friction coefficient μ activated. It should be noted that in this model, particle rotation is restricted if all neighbouring contacts are unbonded to address the lower interlocking forces between grains when using spherical particles.

Particle upscaling

Scaling up the particle size while maintaining the same geometrical dimensions of the problem domain reduces the number of particles in the model. The key to successful upscaling is ensuring that the macro properties (such as Young's modulus and Poisson's ratio) remain unchanged. For this reason, the contact laws must be adjusted to account for the particle scaling factor *S*. The damage model is framed to be scalable by imposing a particle upscaling law for different parameters, as proposed below.

$$\begin{cases} \bar{E}_{mod,S} = \bar{E}_{mod} \\ \bar{\kappa}_S{}^* = \bar{\kappa}^* \\ E_{mod,S} = E_{mod} \\ \kappa_S^* = \kappa^* \\ \sigma_{t,S} = \sigma_t \\ \sigma_{c,S} = \sigma_c \\ C_S = C \\ u_S^c = S u^c \\ \theta_S^c = \theta^c \\ g_{a,S} = S g_a \\ g_{b,S} = S g_b \end{cases} \tag{5}$$

Where, $\bar{E}_{mod}$ and $\bar{\kappa}^*$ are the effective modulus and normal-to-shear stiffness; they are defined as $k_n * l$ and k_n/k_s, respectively. l is the bond length defined as the sum of the radii of the two particles connected by the bond. In addition, the subscript *S* means the value at scale *S*.

The elastic ($\bar{E}_{mod}, \bar{\kappa}^*, E_{mod}, \kappa^*$) and strength ($\sigma_t, \sigma_c, C$) parameters have already been validated as scale independent (Potyondy & Cundall, 2004, Zheng et al. 2022). For softening parameters, Liu et al. (2018) demonstrated that softening is insensitive to particle size. Therefore, a linear upscaling law is proposed for u^c, while the rotational softening parameter θ^c, being a dimensionless variable, remains scale independent. Finally, both the bond activation gap and the far-field interaction gap are assumed to follow a linear scaling law.

On the PFC7.proj

Table 1 DEM damage model parameters for samples with three different upscaling ratios.

S	1	10	100
$\bar{E}_{mod}(E_{mod})$ (GPa)	1	1	1
$\bar{\kappa}^*$ (κ^*)	5	5	5
σ_t (MPa)	1	1	1
σ_c (MPa)	10	10	10
C (MPa)	1	1	1
d_{00} (mm)	6.6e-2	6.6e-1	6.6
u^c (m)	1e-4	0.001	0.01
θ^c (rad)	1e-2	1e-2	1e-2
g_a (mm)	$0.1d_{00}$	$0.1d_{00}$	$0.1d_{00}$
g_b (mm)	$0.4d_{00}$	$0.4d_{00}$	$0.4d_{00}$

The provided example consists in a TX compression simulation. Four .dat files are included, each with extensive comments to ease understanding of this project. **Generate_sample.dat** shows how to generate an unbonded cubic sample enclosed by rigid walls, using a prescribed particle size distribution (PSD), see Zheng & Ciantia (2025). The final sample includes 6891 particles with a porosity of 0.5.

Pb_change.dat can install numerical bonds between untouched particles based on the bond activation gap. Also, this file defines the gap for far-field interaction by setting 'rgap' in the fish code. In addition, strength and softening parameters are assigned to each bond.

Thirdly, **preload.dat** consolidates this bonded sample to reach a target stress level (isotropic compression). In this study, the target stress is 100kPa. This consolidation process is achieved by imposing servo-controlled mechanism on six walls.

Once obtain the pre-consolidated sample**, TX.dat** file assigns vertical velocities to the top and bottom walls, while the left four lateral walls still remain under servo control.

To evaluate the upscaling effect of this linear law, the model is first run with an upscaling factor of 1. Then after exporting the histories and modifying the .p3sav filenames, the mode is re-run with upscaling ratios of 10 and 100. As shown in the following figure, as long as the sample is large enough to be considered as a representative elementary volume (REV), the macro response remains scale independent. The figure also provides scale independence evidence from a micro scale perspective, as similar failure modes caused by local shear bands are observed in all three samples.

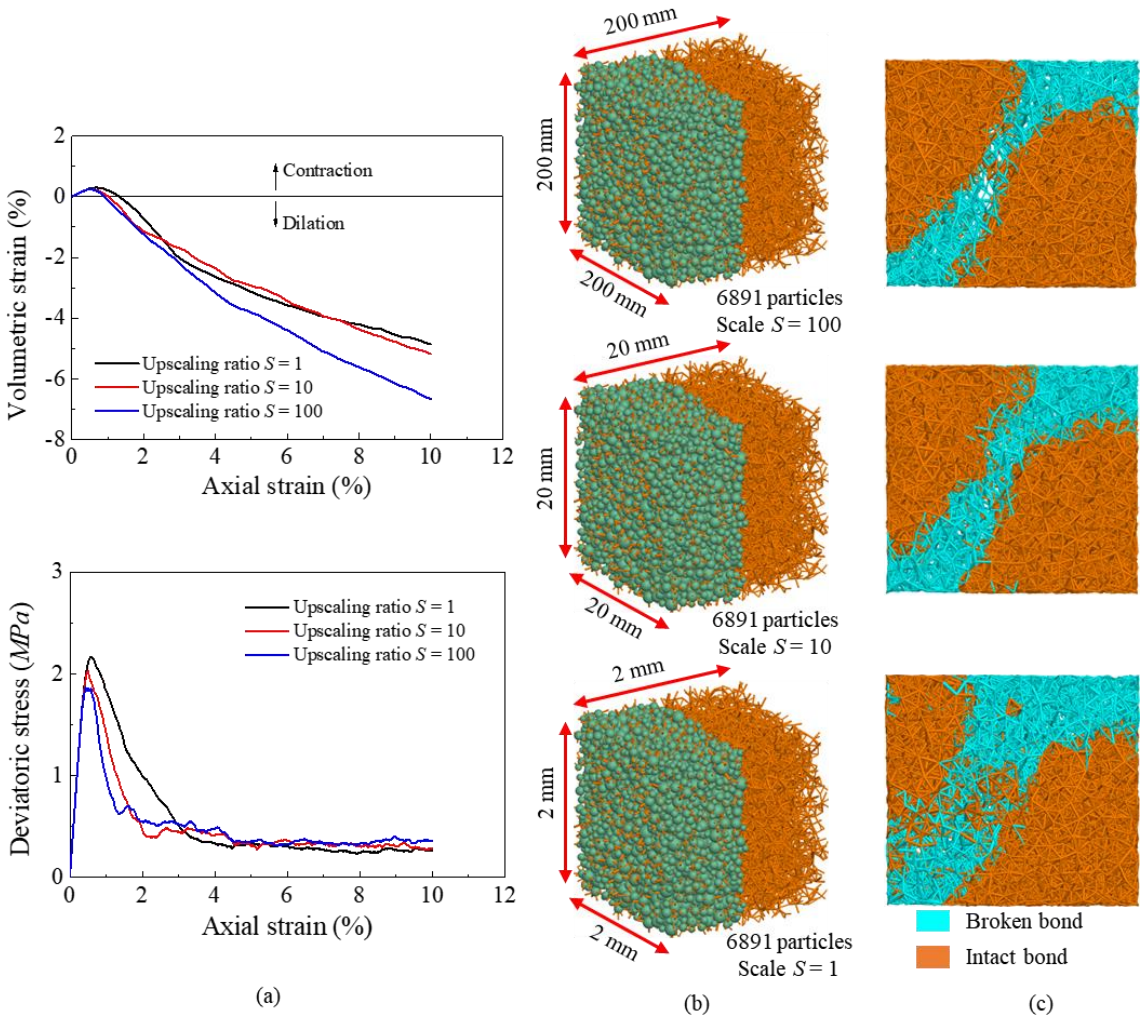

Figure 1 (a) stress-strain macro response of triaxial compression under (100kPa) confinement; (b) snapshot of DEM initial numerical samples and (c) snapshot of damaged and intact bonds at end of shearing showing similar response despite particle scaling.

Reference

Liu, H., Lin, J., He, J. Da, & Xie, H. Q. (2018). Discrete elements and size effects. *Engineering Fracture Mechanics*, **189**: 246–272. https://doi.org/10.1016/J.ENGFRACMECH.2017.11.019

Nguyen, N. H. T., Bui, H. H., Nguyen, G. D., & Kodikara, J. (2017). A cohesive damage-plasticity model for DEM and its application for numerical investigation of soft rock fracture properties. *International Journal of Plasticity*, **98**: 175–196. https://doi.org/10.1016/j.ijplas.2017.07.008

Potyondy, D. O., & Cundall, P. A. (2004). A bonded-particle model for rock. *International Journal of Rock Mechanics and Mining Sciences*, **41(8)**: 1329–1364. https://doi.org/10.1016/j.ijrmms.2004.09.011

Zheng, J., Previtali, M., Knappett, J., et al. (2022). Coupled DEM-FDM investigation of centrifuge acceleration on the response of shallow foundations in soft rocks. In *10th International Conference on Physical Modelling in Geotechnics* (Chung, M., Kim, S. R., Kim, N. R., et al. (eds)). Korean Geotechnical Society, Seoul, Korea, pp. 264–267.

Zheng, J., & Ciantia, M. O. (2025). An efficient damage-plasticity DEM contact model for highly porous rocks. *Rock Mechanics and Rock Engineering*, **Accepted**.